Contents lists available at SciOpen

Food Science and Human Wellness

journal homepage: https://www.sciopen.com/journal/2097-0765

China Food Publishing Co.

Investigating the improvement of rheumatoid arthritis in rats by deer bone protein through the Keap1/Nrf2-regulated ferroptosis signaling pathway based on transcriptomics

Yanlu Li[a], Junxia Ma[a], Ruyi Feng[a], Yanchao Xing[a], Yingshan Jiang[a], Ling Yu[a], Zhongmei He[a,b], Jianming Li[a,b], Yan Zhao[a,b], Kun Shi[a,b], Ying Zong[a,b,*], Rui Du[a,b,c,*]

[a] College of Chinese Medicinal Material, Jilin Agricultural University, Changchun 130118, China
[b] Laboratory of Production and Product Application of Sika Deer of Jilin Province, Jilin Agricultural University, Changchun 130118, China
[c] Key Lab of Animal Production, Product Quality and Security, Ministry of Education, Jilin Agricultural University, Changchun 130118, China

ARTICLE INFO

Article history:
Received 14 October 2024
Received in revised form 13 November 2024
Accepted 16 December 2024

Keywords:
Deer bone protein
Proteomics
Rheumatoid arthritis
Transcriptomics
Ferroptosis

ABSTRACT

Rheumatoid arthritis (RA) is a common long-term autoimmune disease that causes synovial tissue to grow and behave like a tumor when inflammatory factors are present. This can cause joint pain, muscle loss, and other serious problems. Therefore, finding natural anti-RA products and effective treatment strategies is crucial for achieving good prognoses in RA patients. The deer bone is rich in protein, which has the effect of eliminating rheumatism and strengthening muscles and bones. Through multiple gel chromatography purifications, we obtained the deer bone protein (DBP) with a protein content of 76.43%, which was then analyzed using label-free proteomics. Subsequently, an adjuvant arthritis (AA) rat model was established. The ferroptosis pathway was chosen for study based on transcriptomic analysis of AA rat synovial tissue. The molecules with the best docking scores, Nrf2 and Keap1, were then visualized to confirm their validity. Additionally, results from electron microscopy observations, and Western blot (WB) experiments indicated that deer bone protein activates the ferroptosis signaling pathway, alleviating synovial hyperplasia. Therefore, regulating the Keap1/Nrf2 signaling pathway is key to promoting ferroptosis of deer bone protein to improve RA. This study provides new insights into the search for natural foods to improve RA and offers theoretical support for the full development and utilization of Sika deer resources and deer bone products.

1. Introduction

Rheumatoid arthritis (RA) is a systemic autoimmune disease characterized by inflammation of the joint synovial tissues and extra-articular manifestations, leading to joint pain, functional impairment, and even permanent disability, which significantly impacts patients' quality of life and social function[1-3]. Current treatment strategies for RA primarily include conservative treatments (non-pharmacological and pharmacological therapies) and surgical interventions[4]. In terms of pharmacological treatments, previous research found that the combined application of ferroptosis inducer Erastin and tumor necrosis factor inhibitor etanercept can induce ferroptosis in collagen-induced arthritis mice and inhibit the proliferation of synovial fibroblasts, thereby improving RA[5]. Ferroptosis is a form of programmed cell death caused by the accumulation of lipid peroxides due to metabolic abnormalities and other biochemical processes, and it is widely involved in the development of tumors, autoimmune diseases, neurological disorders, and RA[6-8]. According

* Corresponding author at: College of Chinese Medicinal Material, Jilin Agricultural University, Changchun 130118, China
E-mail address: zongying@jlau.edu.cn (Y. Zong), durui197101@sina.com (R. Du)
Peer review under responsibility of Beijing Academy of Food Sciences.

SciOpen Publishing services by Tsinghua University Press

http://doi.org/10.26599/FSHW.2025.9250484.

to current research on ferroptosis-targeted drugs in RA, antirheumatic drugs such as methotrexate (MTX)[9], sulfasalazine (SSP)[10], and cyclophosphamide (CTX) have been shown to possess pro-ferroptotic effects[11]. These suggest that ferroptosis may be associated with the development and treatment of RA[12-13].

Although drugs such as ferroptosis-inducing agents can control the progression of RA to a certain extent, there is still no method to cure the disease completely[14]. Consequently, in order to better intervene and improve RA during the course of chronic disease development, recent research has increasingly focused on non-pharmacological treatments[15-17], particularly the role of diet and nutritional supplements in RA management[18]. Food provides not only energy but also a variety of bioactive compounds. Studies have shown that soy protein, when used as a complementary medical food ingredient alongside medications for RA, can help alleviate pain and improve cytokine levels[19]. Additionally, jellyfish collagen peptides have demonstrated potential in treating osteoarthritis (OA) through the protection and regeneration of knee cartilage[20]. These findings show that proteins from plants and animals may help fight RA by changing immune responses and stopping inflammatory mediators. They also rarely cause side effects. Thus, naturally derived proteins and their derivatives show promising prospects as complementary approaches in the treatment of RA.

Deer bone, derived from the skeletons of sika deer (*Cervus nippon* Temminck) or red deer (*Cervus elaphus* Linnaeus), is rich in proteins. Previous studies have shown that a compound deer bone extract can improve the osteoporosis model in ovariectomized mice[21]. Furthermore, deer bone extracts have been shown to help fight OA by repairing cartilage damage caused by monosodium iodoacetate (MIA) in rat models of OA[22]. Due to the limited development and use of deer bone and its active components, however, no research has yet suggested that deer bone protein (DBP) can help with RA or explained how it works.

Consequently, we isolated and purified the protein from deer bone and subsequently identified and studied it utilizing liquid chromatography-tandem mass spectrometry (LC/MS). We employed adjuvant arthritis (AA) rat models and examined the transcriptome of the synovial tissues from the animals. Molecular docking was employed to align the identified pathway proteins with peptides derived from DBP. This enabled us to exclude significant regulatory proteins such as Nrf2. Subsequently, a series of *in vivo* investigations, including micro-CT, histological analysis, reverse transcription real-time quantitative polymerase chain reaction (RT-qPCR), and Western blot (WB), were performed to investigate the mechanism by which DBP enhances RA. This study offers theoretical support for the use of DBP and other natural products in the treatment of RA, while also providing fresh insights into the production and application of deer bone resources.

2. Material and methods

2.1 Materials and equipments

Sika deer bone samples were purchased from the Haixia Deer Product Distribution Office (Changchun, China). The BCA protein assay kit (P0012) was obtained from Beyotime Biotechnology (Shanghai, China). Hematoxylin (BA-4097) and eosin (BA-4022) staining solutions were purchased from Zhuhai Beso Biotechnology Co., Ltd. (Zhuhai, China). LC-MS grade methanol (MeOH) was purchased from Fisher Scientific (Loughborough, UK). The compound 2-amino-3-(2-chloro-phenyl)-propionic acid was obtained from Aladdin Biochemical Technology Co., Ltd. (Shanghai, China). Anhydrous ethanol, xylene, and neutral balsam were acquired from Sinopharm Chemical Reagent Co., Ltd. (Shanghai, China). Methotrexate (MTX; M813626) was purchased from the Changchun Tianwei Chemical Products Distribution Office (Changchun, China). Ferrostatin-1 (Fer; HY-100579) was obtained from MedChemExpress (Monmouth Junction, USA).

The primary antibody against NRF2 (1:1 000) was purchased from ABclonal Technology (Woburn, USA). Primary antibodies against GPX4 (1:1 000) and HO-1 (1:1 000) were purchased from Chengdu Zen Bioscience Co., Ltd. (Chengdu, China). Primary antibodies against KEAP1 (1:2 000) and ACSL4 (1:2 000) were obtained from Boster Biological Technology Co., Ltd. (Wuhan, China). The primary antibody against SLC7A11 (1:2 000) was purchased from Affinity Biosciences (Liyang, China). The antibody against β-actin and the secondary antibody, goat anti-rabbit IgG (H + L), were purchased from Elabscience Biotechnology Co., Ltd. (Wuhan, China).

Liquid chromatography was performed using an Easy-nLC/Ultimate 3000 system coupled with an Orbitrap Fusion Lumos mass spectrometer and a C_{18} column (1.9 μm, 150 μm × 120 mm), all manufactured by Thermo Fisher Scientific (Waltham, USA). The paraffin embedding machine (Leica EG1140) and rotary microtome (Leica RM2255) were manufactured by Leica Biosystems (Nussloch, Germany). Samples were weighed using an FA1004N electronic balance from Shanghai Precision Scientific Instrument Co., Ltd. (Shanghai, China). Optical microscopy was conducted using an Olympus BX51 microscope (Olympus Co., Tokyo, Japan), and image analysis was performed using the NIS-Elements BR system (Nikon Co., Tokyo, Japan). Micro-computed tomography (micro-CT) scanning was performed using a vivaCT 80 system (Scanco Medical AG, Brüttisellen, Switzerland). Transmission electron microscopy (TEM) images were acquired using a JEM-1400FLASH microscope (JEOL Ltd., Akishima, Japan).

2.2 Preparation of DBP

Fresh Sika deer leg bones were broken down into fragments approximately 2–3 cm in size. After cleansing with deionized water, the bones were immersed in petroleum ether to defat them. Subsequently, the bones underwent demineralization by soaking in a 4% hydrochloric acid solution for 24 h. Once decalcification was complete, the bones were extensively rinsed with deionized water until the pH returned to neutral. Extraction was performed in a water bath at 65 ℃ with a solid-to-liquid ratio of 1:10 (g/mL). This process was repeated three times, with each extraction cycle lasting 3 h. The combined extracts were then centrifuged at 8 000 r/min for 15 min. The supernatant was lyophilized, yielding a light yellow powder referred to as deer bone water extract (DBWE). DBWE was purified by Sephadex G-25 gel filtration chromatography and lyophilized after dialysis to obtain DBP.

2.3 Animal experiments

Healthy female Wistar rats (4 to 8 weeks, 180 to 220 g, SPF) were bought under license number SCXK (JI) 2023–0002 from Yisi Experimental Animal Technology Co. (Changchun, China). All animal experiments have been approved by Jilin Agricultural University's Animal Welfare and Ethics Committee (Ethical Review Acceptance No. 20211011003). The animals were kept in the normal ((25 ± 2) ℃) environment with 12:12 h of light-dark cycle and fed standard basic feed and cold-boiled water. All animal experiments were conducted in accordance with the UK Animals (Scientific Procedures) Act 1986 and associated guidelines, the EU Directive on Animal Experiments 2010/63/EU, and the NIH Guidelines for the Care and Use of Laboratory Animals (NIH Publication No. 8023, revised 1978). All animals were acclimatized to their new environment for 1 week before the start of the study.

2.4 Identification of DBP by liquid chromatography-tandem mass spectrometry (LC-MS/MS)

For sample lysis and protein extraction, an SDT buffer (4% SDS, 100 mmol/L Tris-HCl, 1 mmol/L DTT, pH 7.6) was used, and protein content was performed with a BCA protein assay kit (Bio-Rad, USA). Electrophoresis was conducted at 5 mA/gel for 16.5 h using a buffer containing 25 mmol/L Tris, 192 mmol/L glycine, and 0.1% SDS. Molecular weight markers (10 μL/well) included Bio-Rad's pre-stained Kaleidoscope Standard and HiMark™ Pre-stained Standard (Invitrogen, USA). Gels were stained with Coomassie Blue for 48 h at room temperature.

Samples were separated using a nano-UPLC system with buffers A (0.1% formic acid in water) and B (0.08% formic acid in 80% acetonitrile). Mass spectrometry analysis was performed using an Orbitrap Fusion Lumos (Thermo Scientific) with settings of: 78-min analysis, positive ion mode, precursor ion scan range *m/z* 300–1 400, MS1 resolution 120 000, AGC target 5×10^5, MS1 max IT 50 ms, dynamic exclusion 20 s. For MS2, HCD activation was used with an isolation window of *m/z* 1.6, max IT 35 ms, and collision energy 33 eV.

2.5 Bioinformatics analysis of DBP

Protein and peptide identification were accomplished using a searchable database. For this purpose, the *Cervus canadensis* protein database, obtained from NCBI (*Cervus_canadensis_*GCF_019320065.1_protein.faa) was utilized. The search was conducted with MaxQuant version 2.1.4.0. Gene Ontology (GO) and Kyoto Encyclopedia of Genes and Genomes (KEGG) pathway enrichment analyses were performed utilizing the EBI database and InterProScan version 5.31-70.0.

2.6 Establishment of rats model of RA and grouping

An AA rat model was established based on reported protocols with slight modifications[23]. Healthy female Wistar rats were acclimatized for 7 days. For the AA group, 0.1 mL of complete Freund's adjuvant (CFA) was injected intradermally into the plantar region of the right hind paw, while the control group received an equal volume of saline in the same location. After 7 days, a booster immunization was performed with 0.1 mL of incomplete Freund's adjuvant (IFA) in the same area for the AA group, and an equivalent volume of saline was injected into the control group. The arthritis index (AI) was used for evaluation starting from day 1 post-immunization, assessed every 4 days. The scoring primarily focused on the redness and swelling of the joints post-onset, with a maximum score of 16 points (4 points per limb). A score above 6 indicated successful modeling. The scoring criteria were based on the degree and extent of joint redness and swelling, as well as joint enlargement and deformity, using a scale of 0 to 4: 0, absence of redness or swelling; 1, minimal redness and swelling localized to either the tarsal bone or ankle joint (single area); 2, mild redness and swelling extending from the ankle joint to include the tarsal bone region; 3, moderate degree of redness and swelling that spreads from the ankle joint to encompass the metatarsal bone area; 4, severe redness and swelling that extends from the ankle joint to the metatarsal bone, accompanied by joint stiffness and noticeable deformity.

Based on existing literature, we preemptively included a ferroptosis inhibitor group and the current positive drug for RA, MTX group, to provide a clear contrast[24-25]. The experiment consisted of 6 groups ($n = 6$): control group, AA group, AA + MTX (0.5 mg/kg) group, AA + Fer (1 μmol/L) group, AA + DBP-H (800 mg/kg) group, and AA + DBP-L (200 mg/kg) group. The ferroptosis inhibitor group received the drug *via* intraperitoneal injection, while all other rats were administered the drugs *via* oral gavage, with a dosing volume of 1 mL/100 g per day. Administration began on day 15 after the initial immunization. The control group and AA group received an equivalent volume of saline based on their body weight. The joint swelling of the rats was recorded every 4 days. Treatment lasted for 21 days, and 24 h after the final administration, the rats were anesthetized for orbital blood collection. The spleens, thymuses, synovial tissues, and knee joints were harvested and stored at –80 ℃ for subsequent analyses.

2.7 Analysis of transcriptome in synovial tissue of rats

2.7.1 RNA extraction and identification

RNA sequencing was performed on randomly selected synovial tissue samples from three groups: the control group, the AA group, and the AA + DBP-H group. Total RNA was extracted using Trizol reagent (Sangon, No. B511311). RNA concentrations were measured using the Qubit™ RNA HS Assay Kit (Life Technologies, No. Q32855). Agarose gel electrophoresis was used to assess RNA integrity and check for genomic contamination.

2.7.2 Library construction and sequencing evaluation

The extracted mRNA is enriched using mRNA Capture Beads. Post-bead purification, the mRNA is fragmented at a high temperature. Using this fragmented mRNA as a template, the first strand of cDNA is synthesized within a reverse transcription enzyme mix. During the synthesis of the second strand of cDNA, end repair and A-tailing are also performed. Adapter ligation follows, after which Hieff NGS® DNA Selection Beads are used for purifying the target fragments. The library is then amplified *via* PCR. Finally, sequencing is conducted using the Illumina Novaseq X Plus platform.

2.7.3 GO and KEGG enrichment analysis of differentially expressed genes (DEGs)

Differential expression analysis of RNA was conducted using DESeq2 software, with inter-group comparisons performed using edgeR. Genes/transcripts with a false discovery rate (FDR) < 0.05 and an absolute fold change (FC) ≥ 2 were considered differentially expressed. GO enrichment analysis identified all significantly enriched GO terms among the DEGs. An FDR ≤ 0.05 was applied after correcting the calculated *P*-values for multiple testing. Pathway enrichment analysis revealed metabolic pathways or signaling pathways significantly enriched in DEGs compared to the whole genome background. This pathway-based analysis aids in further understanding the biological functions of the genes.

2.8 Molecular docking analysis

The crystal structures of the proteins ACSL4, GPX4, HO-1, Keap1, Nrf2, and SLC7A11 used for docking were obtained from the PDB database, with PDB IDs: AF-O60488-F1, 6HN3, 1N45, 1ZGK, 7K2A, and 7EPZ respectively. The 3D structures of the 2 peptides with the highest DBP content (SGDRGETGPAGPAGPIGPVGAR and GETGPAGPAGPIGPVGAR) were constructed using PyMOL 2.5.5 and energy minimized under the MMFF94 force field. Molecular docking was performed using HDOCK software. Prior to docking, the receptor proteins were processed with PyMOL 2.5.5 to remove water molecules, salt ions, and small molecules. The docking box was then set to encompass the entire protein structure. Additionally, ADFRsuite 1.0 was utilized to convert the processed short peptides and receptor proteins into the required PDBQT format for HDOCK docking. During docking, the exhaustiveness of the global search was set to 32, with all other parameters kept at their default settings. The docking conformation with the highest absolute score was considered the binding conformation. Finally, the docking results were visualized using PyMOL 2.5.5.

2.9 Micro-computed tomography (Micro-CT)

Bone parameter analysis and 3D reconstruction of the tibial subchondral bone in rats were performed using a micro-CT (Scanco Medical vivaCT80, Switzerland). Scanning was conducted at a voltage of 55 kV, a current of 144 μA, and a resolution of 9 μm. Following the scan, specialized software was used to perform 3D reconstructions of the tibial subchondral bone and the entire knee joint. The tibial subchondral bone was specifically selected for reconstruction and analysis. Parameters including bone mineral density (BMD), bonesurface fraction (BS/BV), bone volume over total volume (BV/TV), trabecular number (Tb.N), trabecular thickness (Tb.Th), and trabecular spacing (Tb.Sp) were calculated from the 3D reconstructions of the selected slices.

2.10 Histopathological examination

Rats were rapidly euthanized and their knees excised under chloral hydrate anesthesia, with care taken to remove soft tissues while preserving the joint capsule. The joint tissues were fixed in 10% neutral buffered formalin (approximately 10 times the volume of the joint) for 24 h. After fixation, they were washed 3 times each with phosphate-buffered saline (PBS) and distilled water, for 20 min per wash. The tissues were then transferred to a 20-fold volume of Ethylenediaminetetraacetic acid (EDTA) decalcification solution. The EDTA solution was replaced weekly, and the process continued for approximately 2 months until no resistance was felt when puncturing the bones, indicating complete decalcification. Thoroughly rinsed with distilled water, the decalcified tissues were bisected along the mid-sagittal plane, dehydrated through a graded series of ethanol washes, and embedded in paraffin to create 5 μm thick sections mounted on glass slides.

Standard hematoxylin and eosin (H&E staining) was applied to evaluate the morphology of the sagittal sections of the knee joints, assessing macroscopic changes such as synovial thickening and roughness, and increased neovascularization. Fresh sections were stained with Safranin O and Fast Green (S&F staining), where fast green staining was applied for 1–5 min, followed by washing to remove excess stain until the cartilage appeared colorless. The sections were then dipped in 1% acid alcohol for 10 s and briefly rinsed with tap water. Safranin O staining was applied for 1–5 s, followed by rapid dehydration through a series of ethanol baths (5, 2, 10 s, and a final microscopic inspection). The sections were cleared in clean xylene for 5 min and mounted with neutral gum. Additionally, Prussian blue staining enhanced by 3,3′-diaminobenzidine (DAB) was used to stain iron particles brown in the suprapatellar synovial tissues. All stained sections were examined under a microscope for image capture and analysis.

2.11 Immunohistochemistry staining

Post-excision of the knee-joints, the treatment regimen adhered to the previously mentioned protocols. Sections embedded in wax underwent dewaxing with hot water and complete coverage with pepsin. For antigen retrieval, the sections were incubated in a 37 °C oven for 30 min, followed by three PBS washes. Endogenous peroxidase activity was quenched using 3% hydrogen peroxide and the samples were then blocked with 3% BSA for 30 min at room temperature. Primary antibodies targeting GPX4, Nrf2, and SLC7A11 were applied and incubated overnight at 4 ℃. Following 3 more PBS washes, the sections were incubated with the secondary antibody for 50 min at room temperature. After additional PBS washes, DAB was used as a chromogen, nuclei were counterstained with hematoxylin, and the sections were dehydrated, mounted, and evaluated microscopically (Nikon). Digital pathology image analysis was conducted using Aipathwell software to quantify the percentage of positively stained cells corresponding to GPX4, Nrf2, and SLC7A11.

2.12 Observation of synovial tissue by transmission electron microscope

Samples were initially fixed with 2.5% glutaraldehyde and then post-fixed with 1% osmium tetroxide. They were dehydrated through a graded series of acetone solutions: 30%, 50%, 70%, 80%, 90%, 95%, and 3 changes of 100%. The specimens were then infiltrated with Epon-812 embedding medium in a stepwise manner using acetone to Epon-812 ratios of 3:1, 1:1, and 1:3, respectively. Pure

Epon-812 was used for the final embedding. Semithin sections were observed under a light microscope, and the synovial regions of the knee joints were selected. Ultrathin sections (ranging from 60 to 90 nm) were sliced and mounted onto copper grids. These sections underwent staining with uranyl acetate for 10 to 15 min, followed by lead citrate staining for 1 to 2 min, both at room temperature. Imaging was conducted utilizing a JEOL-manufactured JEM-1400FLASH transmission electron microscope (Japan). The initial step involved scanning the entire tissue on each grid at low magnification, subsequently focusing on targeted areas for detailed examination of pathological alterations.

2.13 Enzyme-linked immunosorbent assay (ELISA) analysis

The sera and synovial tissue homogenates obtained from section 2.6 were utilized for ELISA assays. Following the protocols specified in the respective kit instructions, the absorbance was measured using a microplate reader (Synergy HTX, BioTek) to determine the levels of interleukin-6 (IL-6), IL-1β, tumor necrosis factor-α (TNF-α), rheumatoid factor (RF, Sino Best Biological Technology Co., Ltd., China), malondialdehyde (MDA, S0131M, Beyotime Biotechnology, China), superoxide dismutase (SOD, S0101M), reduced glutathione (GSH, BC1175, Solarbio Life Science, China), and Ferrous Ion (Fe^{2+}, E-BC-K773-M, Elabscience Biotechnology Co., Ltd., China).

2.14 RT-qPCR analysis

Total RNA was extracted from tissues by TransZol Up Plus RNA Kit (ER501-01) and then reverse transcribed, amplified and RT-qPCR. The specific primer sequences used in this study are listed in Table 1. Finally, relative expression level was quantified by formula $2^{-\Delta\Delta Ct}$.

2.15 WB analysis

Rat synovial tissues were homogenized in a protein lysis buffer and centrifuged at 12 000 × *g* for 15 min at 4 ℃ to isolate proteins. Protein concentration was determined using a BCA assay kit (Beyotime, Shanghai, China). Subsequently, proteins were resolved by SDS-PAGE and transferred to PVDF membranes. These membranes were blocked with 5% non-fat milk for 2 h and then incubated overnight with specific primary antibodies at 4 ℃. Following 3 washes with TBST, the membranes were incubated with the secondary antibody for 2 h at room temperature. Afterward, the membranes were exposed to ECL substrate for 30 s in the dark. Protein bands were visualized using a WB imaging system, and band intensities were analyzed quantitatively with Image J software.

2.16 Statistical analysis

The experimental data were reported in terms of mean ± standard deviation (SD). Statistically significant differences, with a significance level of $P < 0.05$, were evaluated using one-way analysis of variance (ANOVA). The analyses in the study were performed using Origin 8.5 software (Origin Lab Co., MA, USA).

3. Results

3.1 Identification and quantitative results of DBP

The BCA protein assay results showed that the protein content of DBWE was 58.15%, and after purification with Sephadex G-25 gel filtration chromatography, the protein content of DBP rose to 76.43%. SDS-PAGE analysis demonstrated that the majority of the proteins in DBP were within the 15–50 kDa range. LC-MS/MS identified 26 proteins and 69 peptides in DBP (Figs. 1A and B). Tables S1 and S2 provide the detailed lists of all identified proteins and peptides. The top 4 peptides exhibiting the strongest signals in DBP were specifically identified as fragments of the collagen type I alpha 1 chain. Furthermore, we analyzed the distribution of protein coverage and the number of peptides assigned to each protein; proteins with the least sequence coverage were the most numerous (Figs. 1C and E). The length distribution of peptides identified by mass spectrometry after trypsin digestion showed a peak between 10 and 13 amino acids, with 90% of the peptides being 24 amino acids or shorter (Fig. 1D).

3.2 Functional annotation and enriched pathways of DBP

Proteins engage in ten diverse biological processes, among which binding, structural molecule activity, and cellular anatomical entities stand out as the most prevalent, as depicted in Fig. 1F. These proteins underwent KEGG pathway annotation, revealing key signaling pathways such as protein digestion and absorption, ECM-receptor interaction, and the PI3K-Akt signaling pathway, among others, as their major functional routes (Fig. 1G).

Table 1
Tissue RT-qPCR related primer sequences.

Gene	Forward (5′–3′)	Reverse (5′–3′)
GPX4	ACCAGTTCGGGAGGCAGGAG	CACAGTGGGTGGGCATCGTC
Nrf2	ATGCCTTCCTCTGCTGCCATTAG	ACCGTGCCTTCAGTGTGCTTC
HO-1	AGGGTCAGGTGTCCAGGGAAG	TCTGCTTGTTTCGCTCTATCTCCTC
ACSL4	CCGCTTGTGACTTTATATGCTACCC	GCCGCCTTCAGTTTGCTTTCC
SLC7A11	TCATCATCGGCACCGTCATCG	CTCCACAGGCAGACCAGAACAC
KEAP1	GCTGCGAGTCCGAGGTGTTC	CAGGAAGCGTGGCGTGAGAG
GAPDH	CAAGTTCAACGGCACAGTCAAGG	ACATACTCAGCACCAGCATCACC

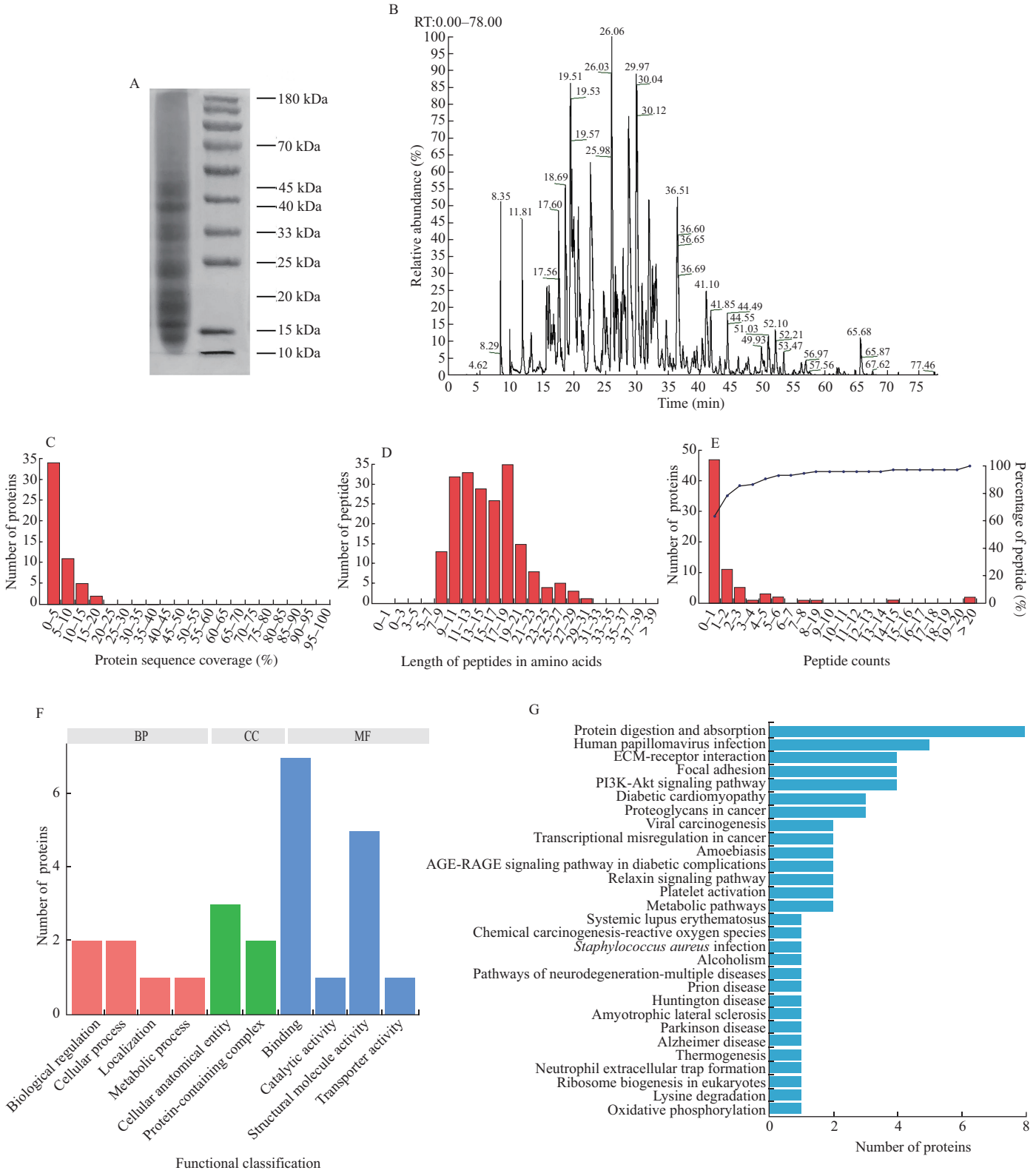

Fig. 1 Identification of DBP, functional annotation, and pathway enrichment. (A) SDS-PAGE results for DBP. (B) Mass spectrum Basepeak of DBHE. (C) Distribution of the proportions of proteins identified for different coverage levels is presented, with the abscissa representing the percentage of identified protein sequence coverage and the ordinate indicating the number of proteins identified. (D) Horizontal axis represents the peptide length, and the vertical axis indicates the number of peptides of corresponding lengths. The peptide length distribution chart demonstrates the length distribution of peptides identified by mass spectrometry following trypsin digestion. (E) Distribution of the number of identified peptides corresponding to the identified proteins. (F) Functional annotation of DBP GO. (G) Notes on the KEGG pathway of DBP proteins.

3.3 General observations in AA rats

An AA rat model was developed to further assess the impact of DBP on RA (Fig. 2A). Compared with the control group, a significant increase in the swelling and the AI of the right hind paw was observed in both the model group and the treatment groups during days 0–14, confirming the successful establishment of the model. From days 15 to 35, after the start of treatment, a marked reduction in the swelling of the right hind paw was observed in both the MTX positive control group and the DBP-treated groups (Figs. 2B and C). Notably, rats in the group receiving the ferroptosis inhibitor *via* intraperitoneal injection showed varying degrees of swelling in both hindpaws, with more pronounced swelling in the right hindpaw. One rat in the MTX group experienced diarrhea, likely due to the hepatotoxic side effects of MTX. In contrast, during the administration of DBP, no abnormalities were observed in the eyes, fur color, feces, respiration, temperature, or behavior. DBP administration resulted in a gradual increase in body weight of the rats (Fig. 2D). Safety evaluation of deer bone extract was carried out in the laboratory beforehand, which showed that it was non-toxic in the dose range[26]. Additionally, compared with the control group, the spleen and thymus indices of rats in the AA group and the AA + Fer group were significantly higher ($P < 0.000\ 1$). Compared with the AA group, the spleen and thymus index decreased in the MTX group (Figs. 2E and F). Compared with the AA group, the spleen and thymus indices of rats in the AA + DBP-H and AA + DBP-L groups were significantly lower.

3.4 Differential gene analysis in transcriptomics

By comparing the early pharmacological effects of high and low doses of DBP in the animal experiments, we found that a high dose of DBP led to better improvement of RA than the low dose. To elucidate the therapeutic mechanism of DBP in rheumatoid arthritis (RA), we performed transcriptomic analysis on synovial tissues isolated from the knee joints of rats in the control, AA, and AA + DBP-H groups. The criteria for identifying differentially expressed genes were set as FDR < 0.05 and fold difference |FC| > 2. By comparing the control group with the DBP group, we identified 932 differentially expressed genes, of which 80 were upregulated and 852 were downregulated. We found 1 480 genes that were differentially expressed between the AA group and the DBP group. Of these, 159 were upregulated and 1 321 were downregulated (Figs. 3A-C). We performed a clustering heatmap analysis of the differentially expressed genes to uncover patterns and trends in gene expression across different groups, providing a foundation for further functional validation (Fig. 3D).

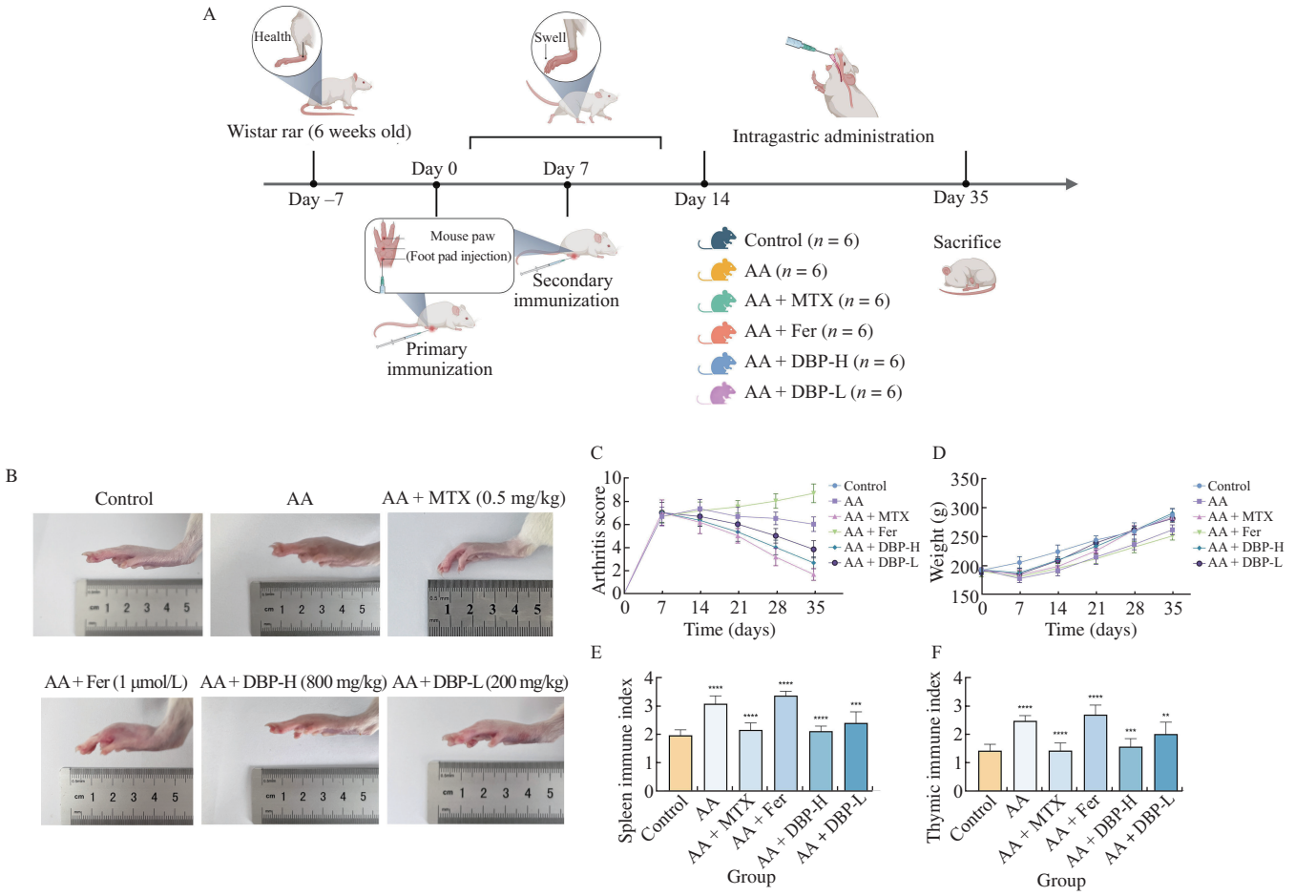

Fig. 2 Establishment of the AA at model. (A) Timeline for the establishment and treatment of AA rats. (B) General observations after treatment in each group. (C) Changes in the AI of rats during the experiment. (D) Body weight changes in rats during the experiment. (E) Spleen immune index. (F) Thymic immune index. $n = 6$, $^{**}P < 0.01$, $^{***}P < 0.001$, $^{****}P < 0.0001$.

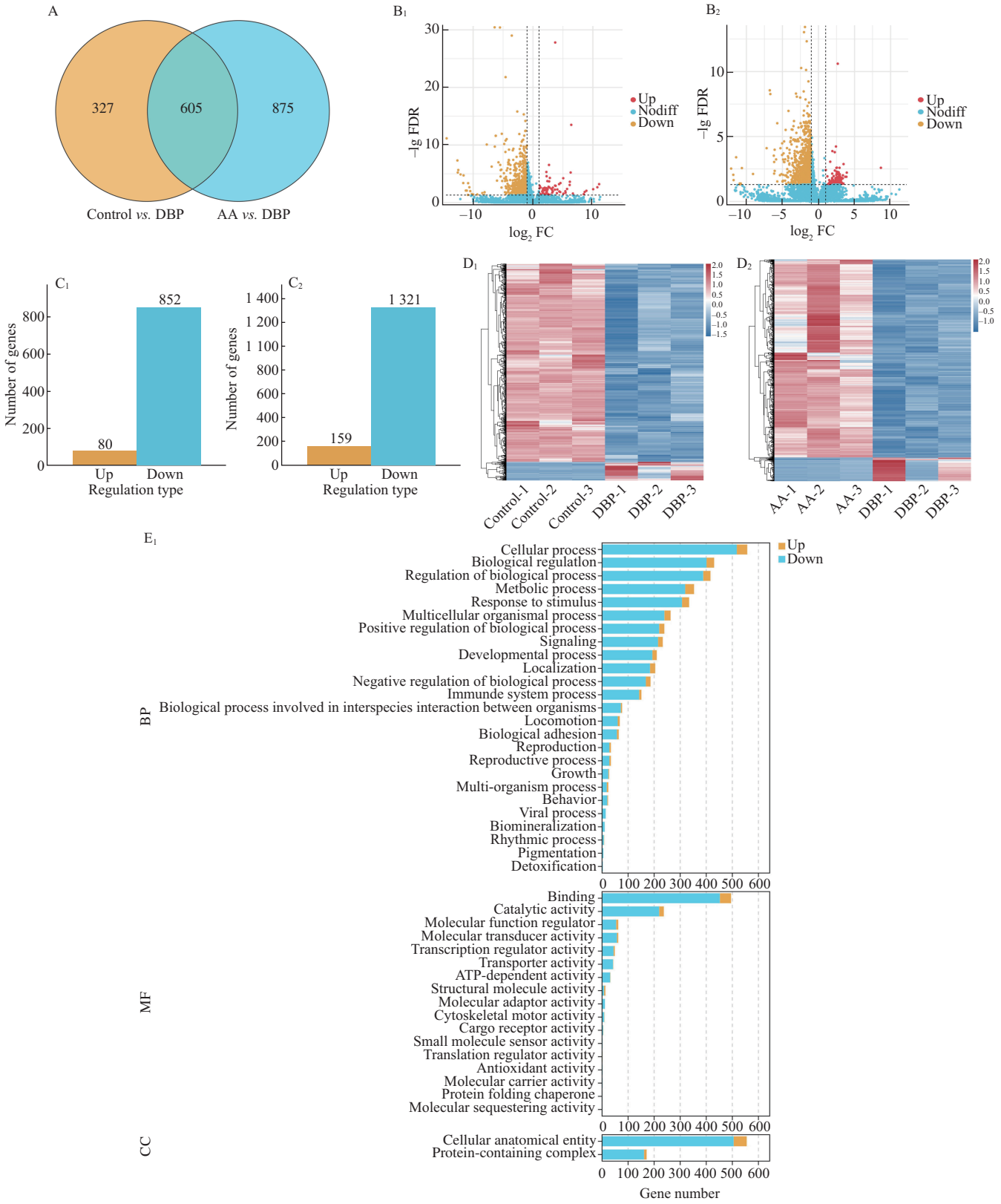

Fig. 3 Results of transcriptome analysis and visualization of molecular docking ($n = 3$). (A) Analysis of differential gene intersections. Differential genes of (B_1) control group *vs.* DBP group, (B_2) AA group vs. DBP group. Genes closer to the ends of the horizontal axis exhibit a greater degree of difference. Difference analysis results of (C_1) control group *vs*. DBP group, (C_2) AA group *vs*. DBP group. DEGs clustering heatmap of (D_1) control group *vs*. DBP group, (D_2) AA group *vs*. DBP group. Enrichment classification analysis was performed on the differential genes of (E_1) control group *vs*. DBP group, (E_2) AA group *vs.* DBP group. DEGs were mapped to GO terms within the categories of MF, CC, and BP in the GO database. Significantly enriched pathways among the DEGs of (F_1) control group *vs.* DBP group, (F_2) AA group *vs.* DBP group. The charts also show the proportion of DEGs and their significance within each pathway category. (G) Visualization of molecular docking of Keap1 and peptide 1 (SGDRGETGPAGPAGPIGPVGAR). (H) Visualization of molecular docking of Keap1 and peptide 2 (GETGPAGPAGPIGPVGAR). (I) Visualization of molecular docking of Nrf2 and peptide 1. (J) Visualization of molecular docking of Nrf2 and peptide 2.

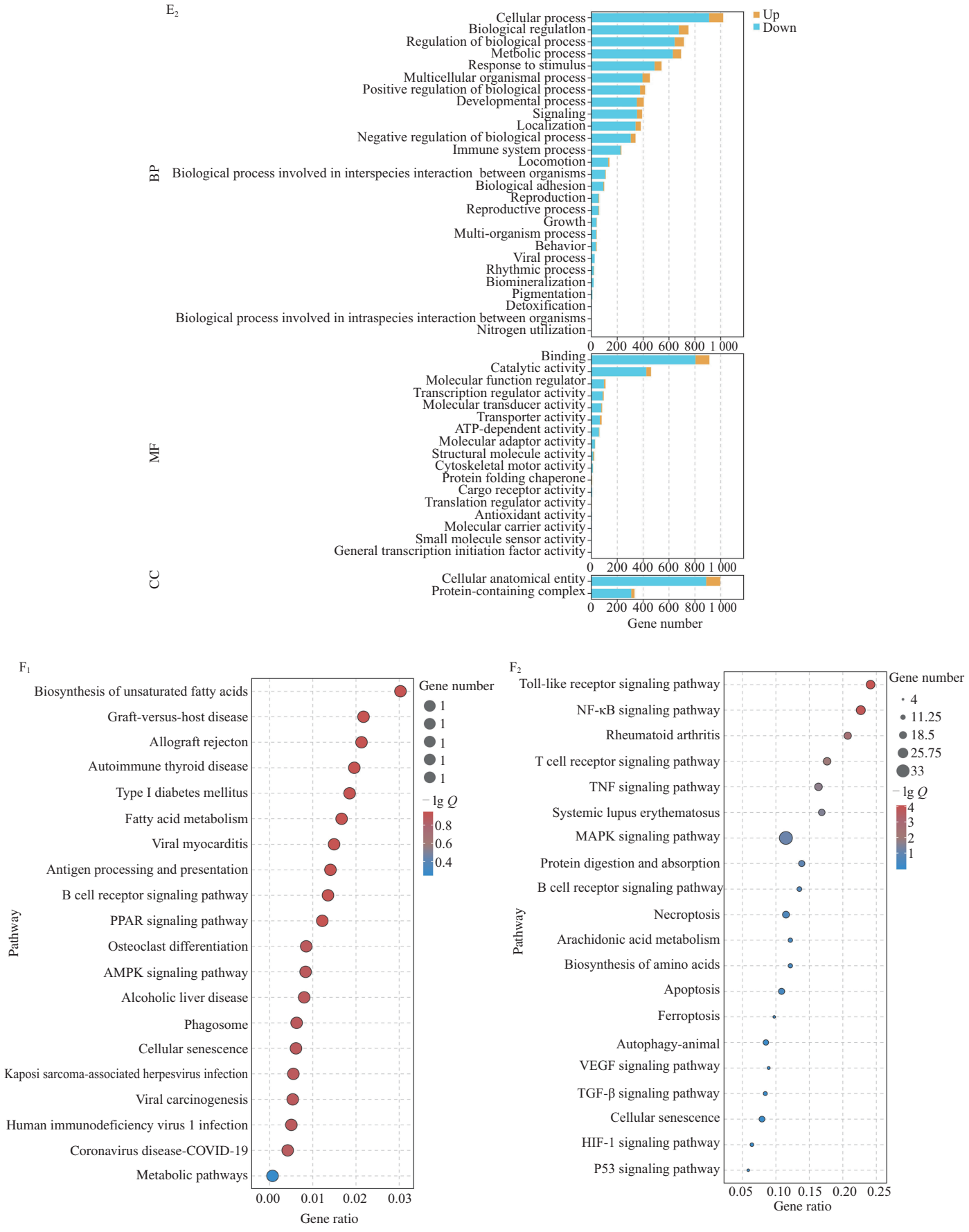

Fig. 3 (*Continued*)

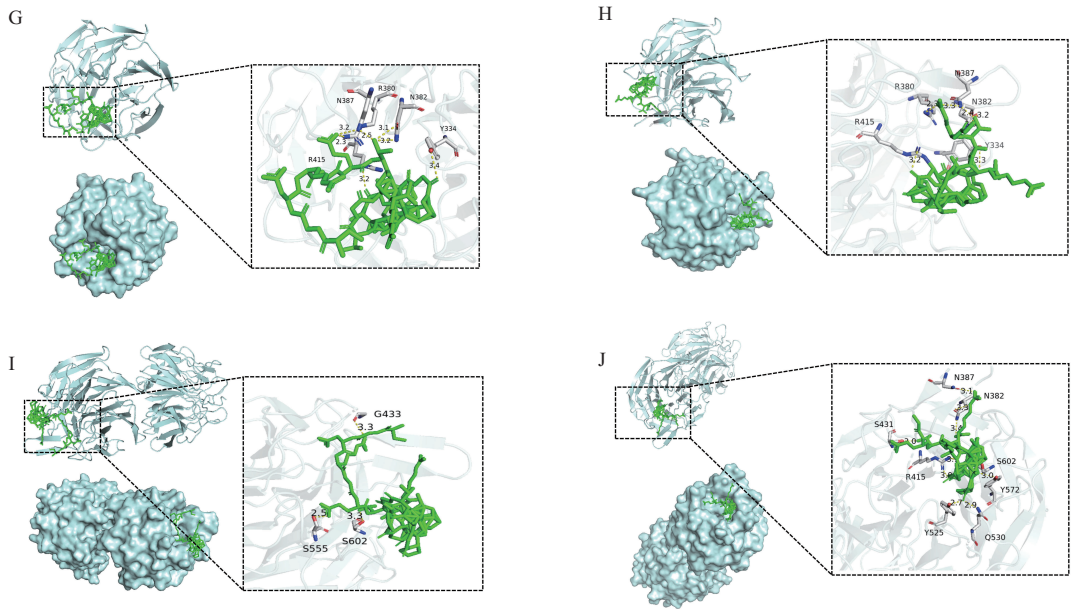

Fig. 3 (*Continued*)

3.5 GO and KEGG enrichment analysis

The most significantly enriched GO terms (Fig. 3E) include biological processes (BP), cellular components (CC), and molecular functions (MF). The GO enrichment analysis of DEGs between the control group and the DBP group, as well as between the AA group and the DBP group, showed that BP primarily focused on cellular processes, biological regulation, and regulation of biological processes; MF mainly centered around binding and catalytic activity; CC primarily centered around cellular anatomical entities and protein-containing complexes. These results suggest that the biological functions of AA rats may be significantly affected.

Combined with KEGG pathway analysis, comparing the control group with the DBP group, a total of 286 pathways were significantly enriched. When comparing the AA group with the DBP group, 311 pathways were significantly enriched. Fig. 3F illustrates the top 20 pathways with the most significant differential enrichment derived from the DEG enrichment analysis. Notably, among the pathways between the AA and DBP groups, in addition to the RA pathway, 2 pathways related to ferroptosis were identified: arachidonic acid metabolism and ferroptosis. These pathways are closely linked to immune system processes, ATP, and antioxidant activities, according to the GO enrichment analysis results. As shown in Table 2, the transcriptomics results indicate that in the ferroptosis pathway, the gene expression of Keap1 and ACSL4 was upregulated in the DBP group compared to the model group. Compared to the control group, the gene expression of Keap1 and ACSL4 was also upregulated in the DBP group. Therefore, DBP may help to remove and break down Nrf2 by increasing the amount of Keap1 in the synovial tissue. Concurrently, the arachidonoyl-CoA biosynthesis catalyzed by ACSL4 promotes ferroptosis by triggering phospholipid peroxidation, thus altering the tumor-like characteristics caused by RA-activated synoviocytes, reducing synovial hyperplasia, and ameliorating RA.

Table 2
Trans per million (TPM) of genes (mean ± SEM, n = 3).

Symbol	Control group	AA group	AA + DBP-H group
Keap1	24.37 ± 0.79	26.25 ± 1.07	33.55 ± 3.12
ACSL4	8.073 ± 0.07	8.04 ± 1.63	12.14 ± 2.08

3.6 Molecular dynamics simulation

Docking simulation technology is a convenient and effective method for investigating the interaction between short peptides and target sites. Supplemental Material 3 presents the docking results of 6 ferroptosis-related proteins with the 2 peptides containing the highest DBP content, resulting in 12 docking sets. Overall, the docking showed good binding affinities. Notably, the docking scores of Nrf2 and Keap1 with both peptides were significantly better than the others, combining the best to reach –371.85. Therefore, we chose to visualize the docking of Nrf2 and Keap1 with these 2 peptides (Figs. 3G-J). It can be seen that each peptide formed excellent hydrogen bonds with the proteins. Hydrogen bonds are one of the strongest types of non-covalent interactions, and the amino acids involved in these hydrogen bonds are key contributors to the binding. The abundance of hydrogen bonds also indicates a very strong binding effect.

3.7 Micro-CT results of knee joint of AA rats

In the field of bone tissue research, Micro-CT enables 2D and 3D imaging observations of bone morphological changes, providing quantitative assessments of bone structure and density, as well as microstructural variations, to characterize bone growth and development levels. Therefore, we observed changes in the microstructure of the knee joints in different groups *via* Micro-CT 3D/2D reconstructed images (Fig. 4A). The results showed that the articular surfaces in the control group were smooth and the structures

were distinct. The knee joints in the AA group displayed hyperplasia and obvious deformities. After treatment with DBP, the damage to the knee joints in the rats was significantly alleviated, with the high dose demonstrating superior efficacy compared to the low dose. Treatment with MTX almost fully restored the knee joints. Additionally, we observed that the hyperplasia and deformity in the AA + Fer group were more severe, suggesting that inhibiting ferroptosis might lead to more severe osteophyte formation in the knee joints. Compared to the control group, the BMD, BV/TV, Tb.N, and Tb.Th were decreased in both the AA and AA + Fer groups, while the Tb.Sp and BS/BV increased, with statistically significant differences ($P < 0.05$). Compared to the AA group, the BMD, BV/TV%, Tb.N, and Tb.Th increased in the AA + MTX and AA + DBP groups, whereas the Tb.Sp and BS/BV decreased (Figs. 4B-G).

3.8 Histopathological test results

Through observation of H&E staining, it can be noted that compared to the control group, the synovial tissue in the knee joints of the AA group and the Fer group showed significant thickening, with a large number of inflammatory cells visible in the lining layer and sub-lining layer. Under high-power magnification, the main cell types observed were synoviocytes, lymphocytes, and neutrophils. In the DBP-L group, H&E staining showed that the synovial tissue of the right knee was still thickened, with prominent pannus and a significant presence of inflammatory cell infiltration. Under high-power magnification, lymphocytes were predominantly observed. The DBP-H group and the MTX group had a smoother surface of the articular cartilage compared to the AA group. They also had much less synovial hyperplasia and more normal joint inflammation (Fig. 4H).

The results of the S&F staining showed that the synovial tissue in the control group exhibited a normal tissue structure, with evenly distributed collagen fibers and clear tissue layers. In contrast, the synovial tissue in the AA group and the Fer group displayed abnormal structural changes, including excessive proliferation of collagen fibers, disorganized tissue structure, and evident inflammatory responses. In the DBP-L group, although some degree of synovial thickening and collagen deposition was still observable, the extent of inflammatory cell infiltration was reduced compared to the AA group. In the DBP-H group and the MTX group, the structure of the synovial tissue was closer to normal, with reduced collagen fiber deposition and a markedly alleviated inflammatory response. This indicates that DBP-H and MTX treatment can effectively improve the pathological condition of the synovial tissue and reduce inflammation (Fig. 4H).

After Prussian blue staining using the DAB method, areas containing iron within the synovial tissue appeared brownish-black, while cell nuclei stained light blue. It was observed that the synovial lining layer in the DBP group and the MTX group showed a significant deposition of iron particles. In contrast, the AA group and the Fer group exhibited synovial hyperplasia and changes in joint structure, with very little iron particle deposition in the synovial lining layer. This suggests that the synovial tissue in the DBP and MTX groups experienced substantial iron deposition, leading to ferroptosis, which in turn reduced synovial hyperplasia and improved RA (Fig. 4H).

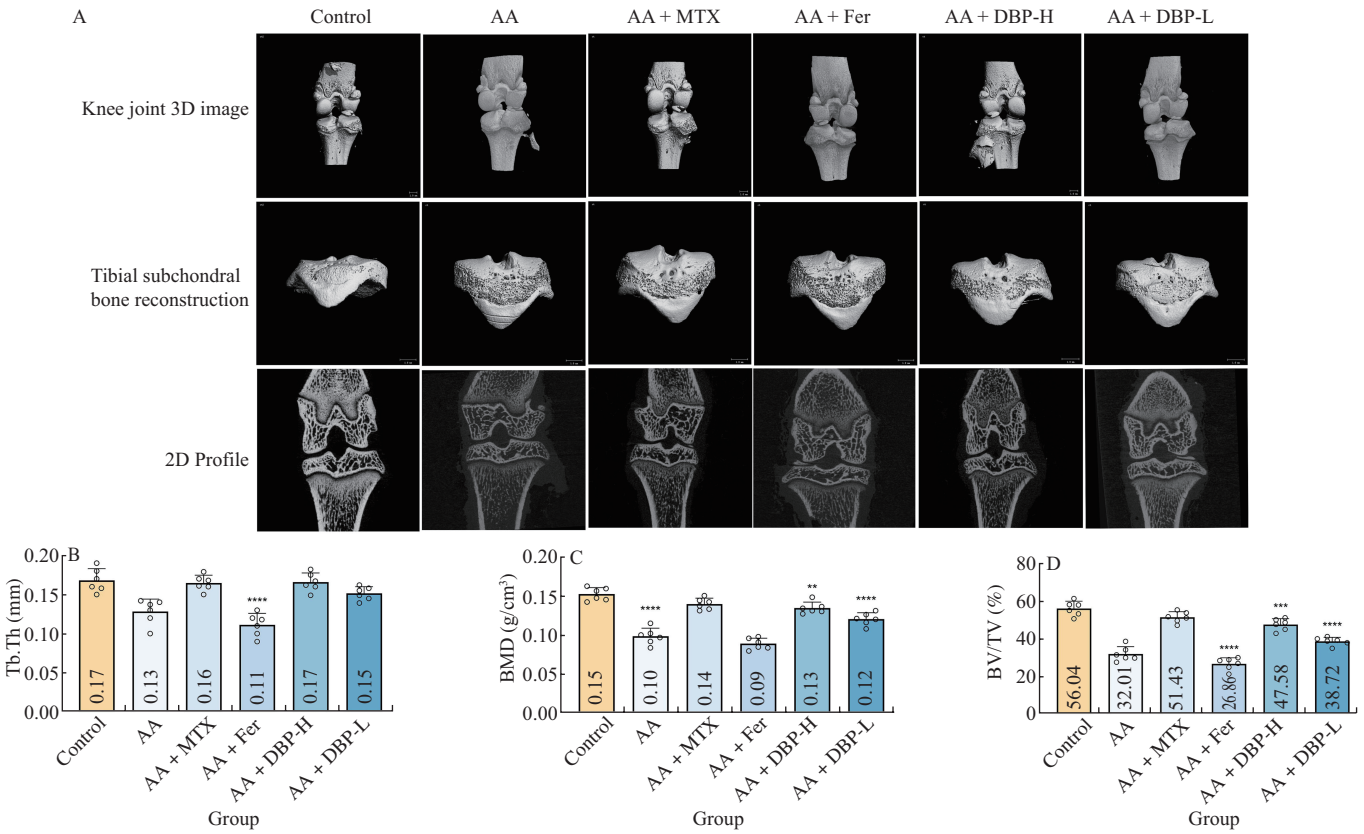

Fig. 4 Microscopic observation and histopathological examination. (A) Reconstruction of tibial subchondral bone and 3D/2D Micro-CT images of knee joints in rats. (B-G) Bone parameter analysis (Tb.Th, BMD, BV/TV, BS/BV, Tb.Sp, and Tb.N), $n = 3$, (H) Histological staining results of the knee joints in rats (H&E staining, S&F staining, and Prussian blue staining). $^{**}P < 0.01$, $^{***}P < 0.001$, $^{****}P < 0.000\ 1$.

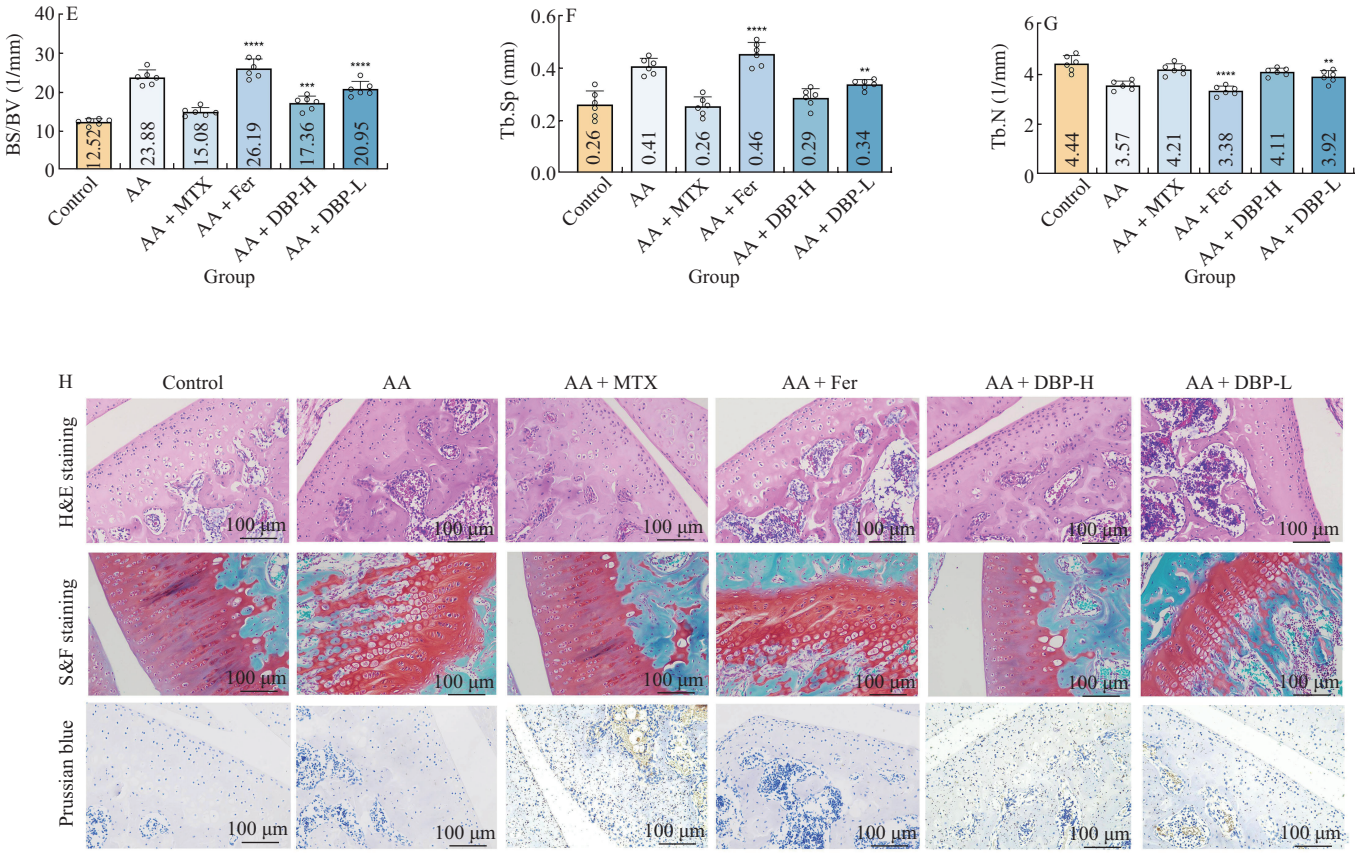

Fig. 4 (*Continued*)

3.9 DBP induced ferroptosis in the synovium of AA rats

In addition to the ferroptosis-related proteins Keap1 and ACSL4 that were already mentioned from the transcriptomic response, we also did immunohistochemical experiments on GPX4, Nrf2, and SLC7A11. We aimed to achieve more comprehensive verification in *in vivo* experiments (Fig. 5A). The immunohistochemistry results demonstrate that the expression of inflammatory markers in the AA group and AA + Fer group was significantly elevated, with the percentage of positive cells for GPX4, Nrf2, and SLC7A11 markedly higher than in the control group ($P < 0.001$). The MTX and DBP groups had less inflammatory cell infiltration, and immunohistochemistry showed very few positively stained cells. The percentage of positively stained cells was also lower than in the AA group ($P < 0.05$, $P < 0.01$). The DBP-H group had a lower percentage of positive cells compared to the DBP-L (Figs. 5B-D). This indicates that under the influence of RA, the immune response in the synovial tissue is intensified, leading to increased infiltration of inflammatory cells and release of inflammatory mediators. When RA activates fibroblast-like synoviocytes, they grow in a way that looks like a tumor. This stops ferroptosis from happening and instead leads to synovial hyperplasia. These changes may contribute to further damage to joint tissue and the progression of the disease. However, the DBP group can facilitate the occurrence of ferroptosis and reduce inflammatory cell infiltration.

3.10 Effects of DBP on mitochondria and other organelles

Observations using transmission electron microscopy (TEM) of synovial tissues allow for a detailed evaluation of intracellular structural changes (Fig. 5E). In the control group, the structure of the synovial cells remains intact, with normal morphology of organelles such as mitochondria and endoplasmic reticulum, and no significant signs of cell damage or apoptosis are observed. However, in the AA group and Fer group, synoviocytes activated by RA do not exhibit characteristics of cellular damage but rather show abnormal conditions such as cell deformation and proliferation. Conversely, in the DBP group and MTX group, inflammatory infiltrated synoviocytes display evident cellular damage, including mitochondrial swelling, expansion of the endoplasmic reticulum, and rupture of the cell membrane associated with ferroptosis. Notably, the phenomenon of ferroptosis is more pronounced with high doses of DBP compared to lower doses.

3.11 Effect of DBP on serum inflammatory factors in AA rats

As depicted in Fig. 6A, compared to the blank control group, the serum levels of RF, TNF-α, IL-1β, and IL-6 in rats within the AA and Fer groups were significantly elevated ($P < 0.000\ 1$). Relative to the AA group, the MTX group demonstrated a significant inhibition of RF and multiple inflammatory mediators in the rat serum ($P < 0.05$).

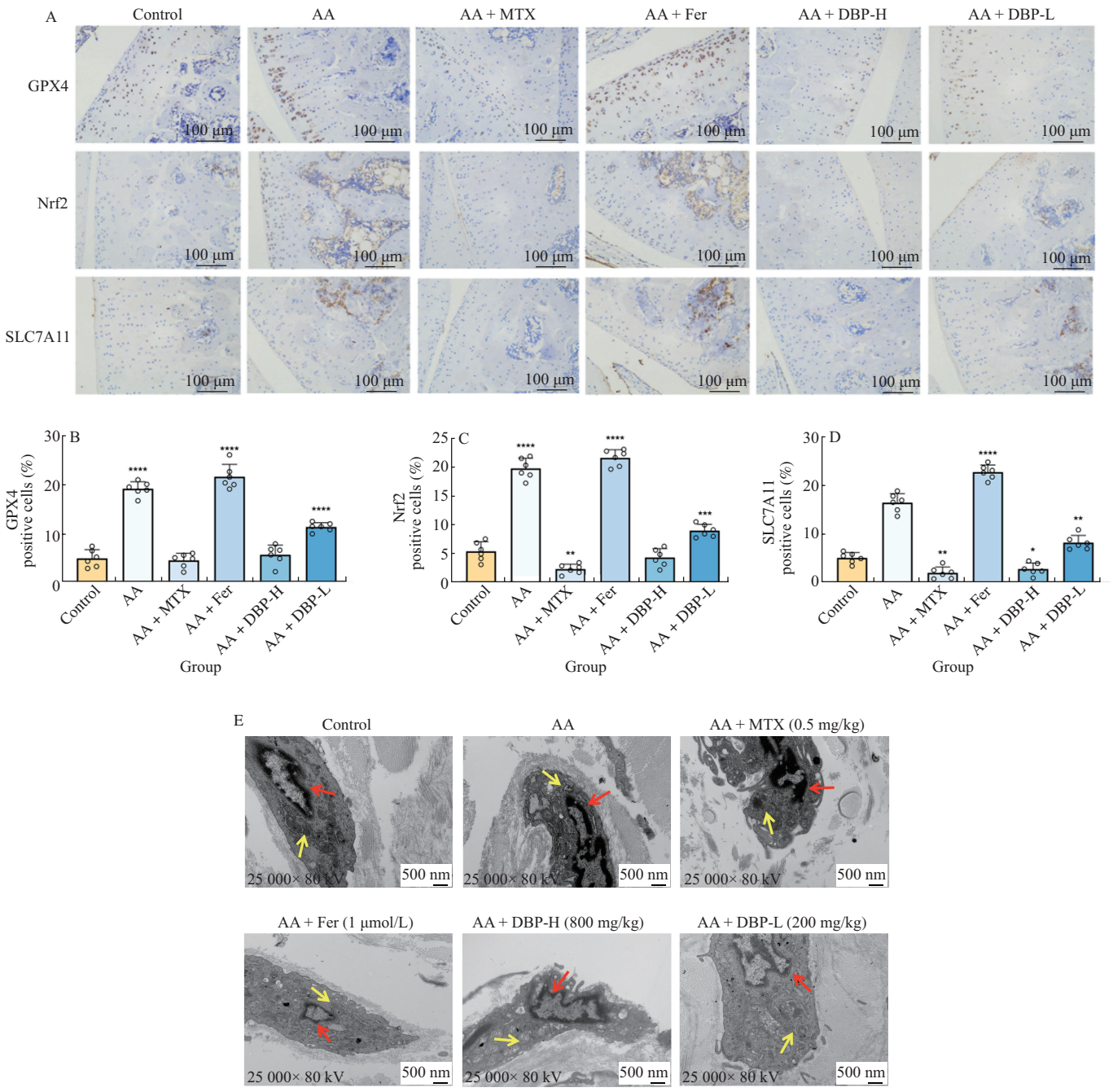

Fig. 5 DBP induced ferroptosis in the synovium of AA rats. (A) Immunohistochemical staining of GPX4, Nrf2, and SLC7A11 in rat knee joints. (B-D) Positive cell rates corresponding to immunohistochemical staining for GPX4, Nrf2, and SLC7A11 ($n = 3$). (E) TEM observation of synovial tissue (scale bar = 500 nm, $n = 3$). Red arrows indicate nuclei, and yellow arrows indicate mitochondria. *$P < 0.05$, **$P < 0.01$, ***$P < 0.001$, ****$P < 0.000\ 1$.

Similarly, the DBP treatment groups influenced the levels of various inflammatory mediators in the serum, significantly suppressing TNF-α, IL-1β, and IL-6 while also reducing the concentration of RF ($P < 0.05$). Furthermore, the AA + DBP-H group exhibited superior effects compared to the AA + DBP-L group. These results suggest that DBP may alleviate inflammatory responses associated with RA by modulating these key inflammatory mediators, thereby exerting a beneficial effect on RA. Additionally, these findings support the potential of DBP as a health food supplement with anti-rheumatic and immunity-enhancing properties.

3.12 Effects of DBP on ferrous ion content and antioxidant capacity in synovium of AA rats

To further validate that the therapeutic improvement in AA rats treated with DBP was attributable to the modulation of ferroptosis in hyperproliferative synovial tissue, we quantified tissue ferrous ion levels and assessed antioxidant capacity (Fig. 6A). The results indicate that, compared to the control group, the AA group also produced a modest amount of ferrous ions. However, the AA + Fer group showed a reduction in ferrous ion levels compared to the AA group. In contrast, the MTX and DBP groups experienced an

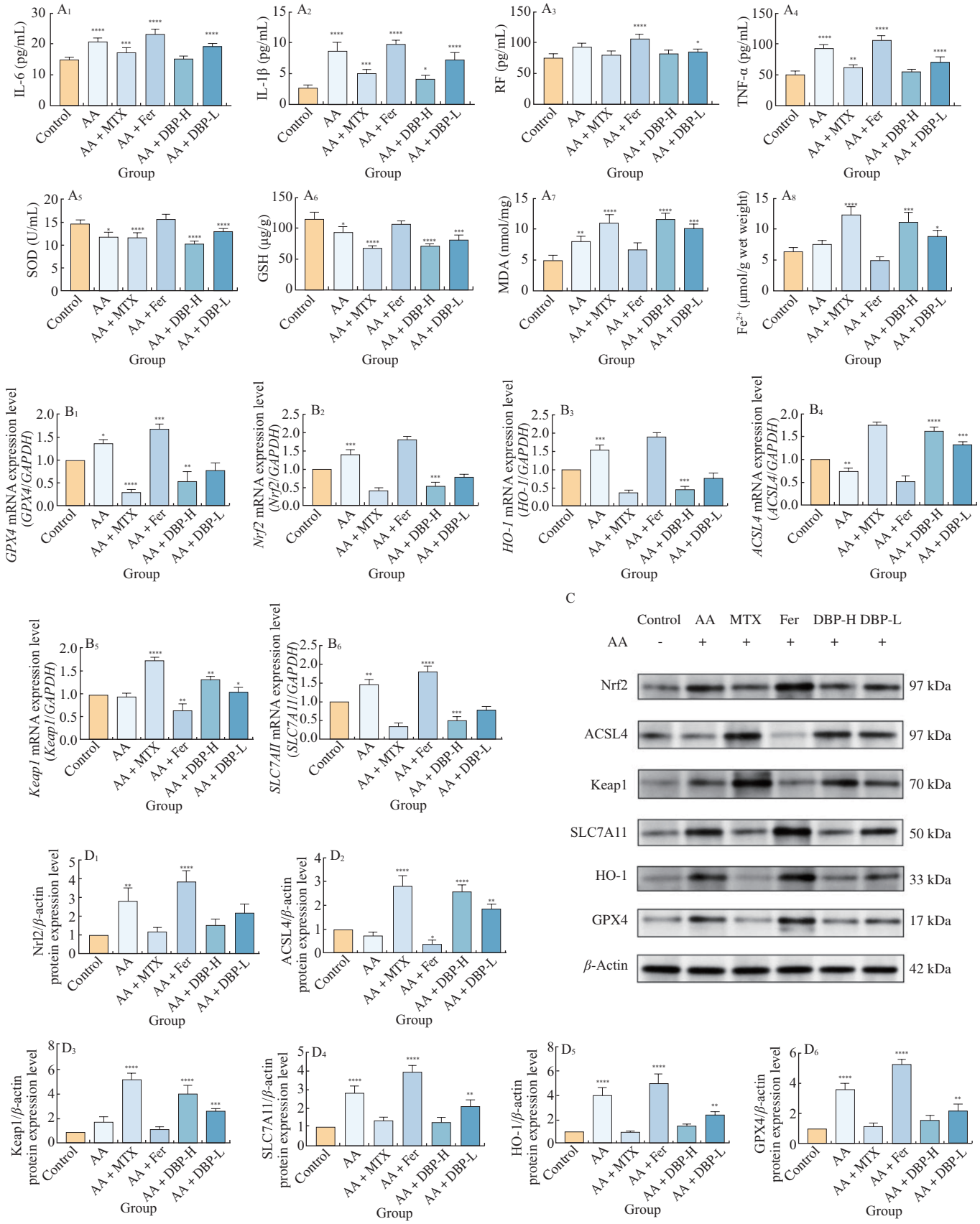

Fig. 6 Effects of DBP on inflammatory cytokines, antioxidant indicators, and ferroptosis-related proteins in the serum and synovial tissue of rats. Impact of DBP on inflammatory cytokines (A_1) IL-6, (A_2) IL-1β, (A_3) RF, (A_4) TNF-α, antioxidant indicators (A_5) SOD, (A_6) GSH, (A_7) MDA and (A_8) Fe^{2+} in the serum and synovial tissue of rats. Effects of DBP on the mRNA expression of (B_1) *GPX4*, (B_2) *Nrf2*, (B_3) *HO-1*, (B_4) *ACSL4*, (B_5) *Keap1*, and (B_6) *SLC7A11* in the synovial tissue of rats. (C) WB results for protein. (D) Immunoblotting grayscale analysis of (D_1) Nrf2, (D_2) ACSL4, (D_3) Keap1, (D_4) SLC7A11, (D_5) HO-1, and (D_6) GPX4. $n = 3$. $^*P < 0.05$, $^{**}P < 0.01$, $^{***}P < 0.001$, $^{****}P < 0.0001$.

accumulation of ferrous ions ($P < 0.001$), with the AA + DBP-H group accumulating more ferrous ions than the AA + DBP-L group. This suggests that both DBP and MTX promote ferroptosis in the inflamed synovial tissue. Furthermore, the synovial tissue in the AA and Fer groups exhibited oxidative stress due to inflammatory infiltration. Since low concentrations of reactive oxygen species (ROS) can induce cell proliferation, this reflects the abnormal state induced by RA activation, thereby exacerbating synovial hyperplasia[27-29]. In contrast, the MTX and DBP groups showed a significant decrease in SOD and GSH, alongside a substantial increase in MDA, thereby reducing the antioxidant capacity of the synovial tissue. This leads to an overproduction of ROS, causes cell apoptosis, which reduces abnormal synovial hyperplasia and improves RA ($P < 0.001$).

3.13 DBP regulates the expression of ferroptosis-related protein to improve AA rats

Subsequently, we utilized RT-qPCR and WB to examine the impact of DBP on the expression of ferroptosis-related proteins (Nrf2, ACSL4, Keap1, SLC7A11, HO-1, and GPX4) in the synovial tissue of AA rats. As shown in Figs. 6B-D compared to the control group, the AA group had lower levels of *ACSL4* and *Keap1* mRNA. On the other hand, Nrf2, SLC7A11, HO-1, and GPX4 protein and mRNA expression were significantly higher. Compared to the AA group, the mRNA and protein levels of ACSL4 and Keap1 were elevated in the MTX and DBP groups, whereas the expression of Nrf2, SLC7A11, HO-1, and GPX4 was significantly reduced ($P < 0.001$). These findings indicate that DBP promotes ferroptosis in a dose-dependent manner, inhibits synovial hyperplasia, and improves RA under pathological conditions.

4. Discussion

RA is a systemic inflammatory autoimmune disease whose precise etiology remains incompletely elucidated[30]. Current clinical medications do not completely cure RA, and there is an urgent need to develop a new therapeutic strategy[31]. Research indicates that RA, a chronic condition, manifests symptoms of bone erosion within 2 years without prompt intervention and treatment. Consequently, the development of pertinent functional foods as a non-pharmacological approach through dietary consumption may mitigate and impede the progression of RA[32].

This study involved the extraction and purification of DBP from deer bone, achieving a protein content of 76.43%. We systematically examined the protein fractions of DBP and its mechanism of action in ameliorating RA through label-free proteomics, animal experiments, transcriptomics, molecular docking, and other relevant experimental methodologies. We identified 26 proteins and 69 peptides from DBP, with 72.46% of the peptides originating from collagen, which is essential for preserving the mechanical properties of articular cartilage and the stability of the extracellular matrix[33-34]. Subsequent bioinformatics analysis corroborated this finding, and the KEGG pathway annotated significant signaling pathways, including protein digestion and absorption, ECM-receptor interactions, among others, which are intricately associated with cartilage repair and joint stability[35]. This establishes the material basis for DBP as a functional food to enhance RA.

To elucidate the mechanism by which DBP mitigates RA, we conducted animal research, successfully establishing a rat model of AA, and performed transcriptome analysis on rat synovial tissue. The results revealed that there were 2 pathways related to ferroptosis in the enrichment pathway of differential genes in AA and DBP groups: arachidonic acid metabolism and ferroptosis pathway. Moreover, the gene expression of *Keap1* and *ACSL4* were up-regulated in DBP group compared with the control group, suggesting that the molecular mechanism of DBP to relieve RA might be related to it. Consequently, we promptly validated the molecular docking of 6 pivotal proteins in the ferroptosis pathway with 2 of the most prevalent deer bone collagen peptides. Following the screening process, the 2 most effective binding proteins identified were Keap1 and Nrf2. Prior research indicates that Keap1 associates with and directs Nrf2 for ubiquitination and subsequent proteasomal destruction under normoxic circumstances, functioning as a sensor and bridging protein[34,36]. Nrf2 is a prominent transcription factor integral to antioxidant defense. Its downstream targets encompass HO-1, Nqo-1, phase II detoxification enzymes including GSHS-transferase, GPX4, GSH reductase, and glutamate-cysteine ligase subunits, alongside various transport proteins linked to multidrug resistance[37]. Ibuprofen, a widely used nonsteroidal anti-inflammatory and anti-RA drug, can then induce glioblastoma cell death by inhibiting the expression of GPX4 and SLC7A11 through down-regulation of the Nrf2 pathway[38]. Therefore, Nrf2 is considered to be an important regulator of pro-iron action[39]. The activity of Nrf2 is tightly regulated by Keap1[40]. In conditions of oxidative stress or elevated levels of electrophilic substances and cytotoxic agents, Nrf2 separates from its binding site on Keap1 and swiftly relocates to the nucleus. Thereafter, Nrf2 associates with antioxidant response elements (AREs) in the promoter region, initiating a cascade of transcriptional pathways to mitigate oxidative stress and preserve intracellular redox homeostasis[41-43]. Therefore, based on the foregoing processes, we predicted that DBP may regulate ferroptosis through the Keap1/Nrf2 signaling pathway and thereby prevent the progression of RA.

This mechanism offers a novel insight into the potential function of DBP in the management of RA; however, additional *in vivo* experiments are required. In the animal experiments, to better compare with the current anti-rheumatic drugs and to clarify the mechanism of DBP in improving RA, we set up a positive MTX group and a ferroptosis inhibitor Fer group, in addition to the conventional control, modeling, and drug administration groups. Simultaneous tests were conducted on the subsequent histological evaluations, micro-CT analysis, inflammatory variables, and further assays. The results indicated that DBP exhibited significant enhancement of RA, ameliorated synovial hyperplasia and inflammatory cell infiltration, improved bone parameter alterations, and markedly decreased the expression of inflammatory factors such as IL-6 and RF in comparison to the AA group. It is worth noting that DBP has a better effect on reducing inflammatory factors compared to MTX. Individual rats in the MTX group showed diarrhea symptoms, suggesting that MTX may have side effects such as hepatotoxicity and lung injury[44]. While DBP is not as effective as MTX in improving RA, it has less toxicity. This makes DBP more suitable for use as a functional food to assist in the treatment of RA. Furthermore, Prussian blue staining, immunohistochemistry for GPX4, SLC7A11, Nrf2, ferrous ions, antioxidant indices, RT-qPCR validation, and

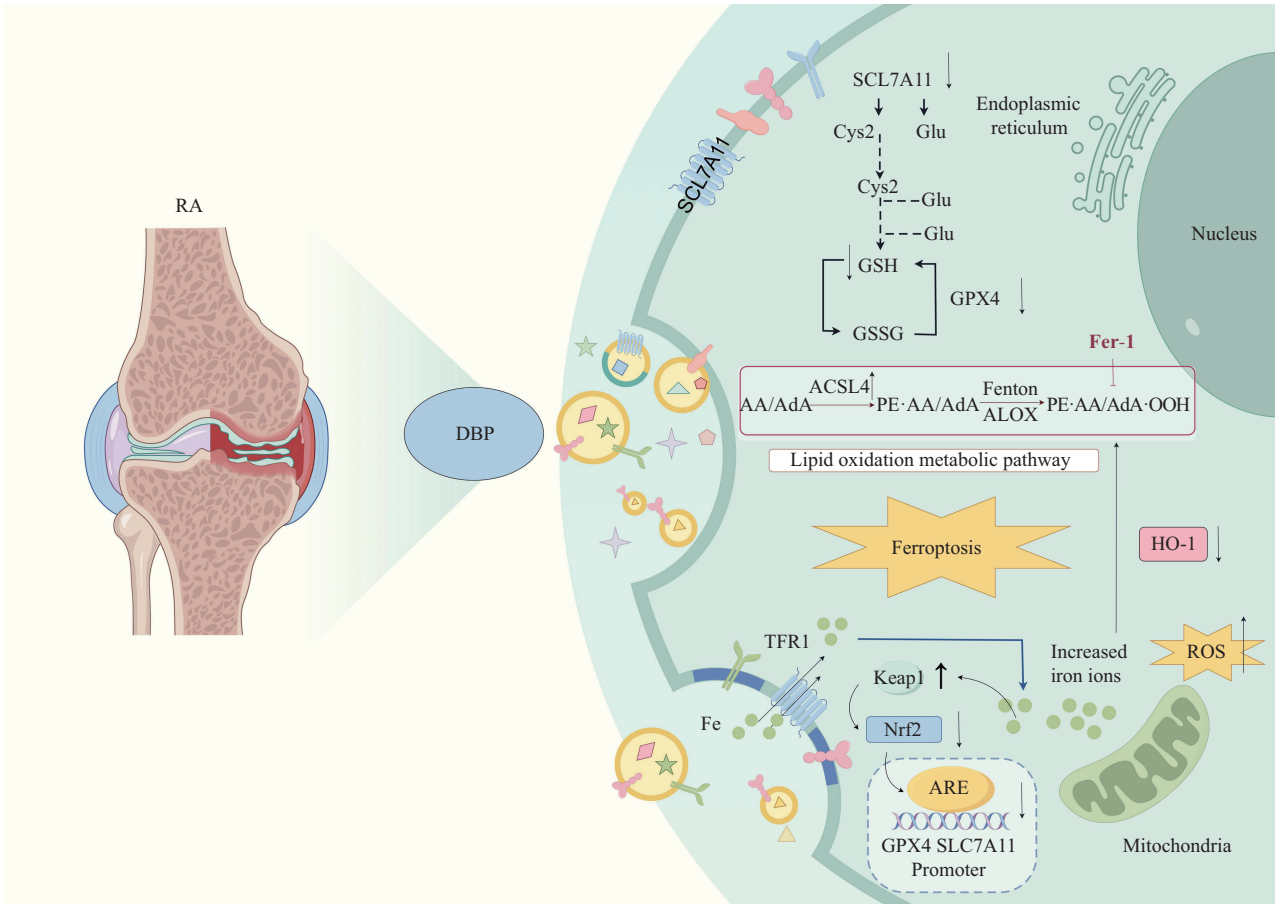

Fig. 7 Mechanism of DBP in regulating ferroptosis pathways to ameliorate RA (By Figdraw).

WB analysis demonstrated an increase in ferrous ions, heightened iron deposition, and elevated MDA levels in the DBP and MTX groups relative to the AA group, which induced oxidative stress in the inflammatory FLS cells, culminating in ferroptosis and thereby mitigating synovial proliferation. Simultaneously, the mRNA and protein concentrations of ACSL4 and Keap1 were increased. In contrast, immunohistochemistry showed a significantly lower rate of positive cells, a decrease in SOD and GSH levels, and a significant decrease in mRNA and protein expression of Nrf2, SLC7A11, HO-1, and GPX4. Ferroptosis features, such as crumpling and rupture of apparent mitochondrial ridges, were also observed by TEM in the DBP group. It has been shown that MTX, the most commonly used DMARD in RA, observed iron overload and ROS accumulation, as well as an increase in FTH1 and a decrease in NCOA4 when treating the hippocampal HT22 cell line[45], which coincides with our finding that MTX promotes ferroptosis. Interestingly, the ferroptosis inhibitor group showed completely opposite results compared to the DBP group, previous studies have demonstrated that ferroptosis inducers can be used as promising anti-RA agents[46], then our validation results precisely suggest that ferroptosis inhibitors, given alone, have a more negative effect on pathologies, such as synovial hyperplasia.

DBP facilitates ferroptosis in the synovial tissues of AA rats, mitigates synovial hyperplasia, and enhances the progression of RA by generating Keap1 overexpression, which subsequently reduces Nrf2 levels (Fig. 7). In view of this, the development of complementary functional foods such as DBP as a supplement to existing therapeutic means is of great significance for improving the symptoms of RA patients and inhibiting the further progression of the disease, and it also provides a scientific basis for the development and resource utilization of deer bone functional foods. The investigation into how DBP modulates ferroptosis to alleviate RA offers a robust scientific foundation for the treatment of RA.

Conflict of interest

The authors declare that they have no known competing financial interests or personal relationships that could have appeared to influence the work reported in this paper.

Data availability

The original contributions presented in the study are included in the article, further inquiries can be directed to the corresponding author.

Acknowledgements

This work was supported by funding from the Major Science and Technology Projects in Jilin Province (20220304001YY, 20220304003YY).

Appendix A. Supplementary data

Supplementary data associated with this article can be found, in the online version, at http://doi.org/10.26599/FSHW.2025.9250484.

References

[1] P. Brown, A.G. Pratt, K.L. Hyrich, Therapeutic advances in rheumatoid arthritis, BMJ 384 (2024) e70856. https://doi.org/10.1136/bmj-2022-070856.

[2] F. Zhang, A.H. Jonsson, A. Nathan, et al., Deconstruction of rheumatoid arthritis synovium defines inflammatory subtypes, Nature 623 (7987) (2023) 616-624. https://doi.org/10.1038/s41586-023-06708-y.

[3] J. Mucke, M. Krusche, G.R. Burmester, A broad look into the future of rheumatoid arthritis, Ther. Adv. Musculoskelet. Dis. 14 (2022) 1759720X221076211. https://doi.org/10.1177/1759720X221076211.

[4] I. Janssen, E. Shiban, B. Meyer, Cervical spine involvement in rheumatoid arthritis: diagnostics and treatment of instability due to rheumatism, Z. Rheumatol. 77 (10) (2018) 889-895. https://doi.org/10.1007/s00393-018-0564-9.

[5] J. Wu, Z. Feng, L. Chen, et al., TNF antagonist sensitizes synovial fibroblasts to ferroptotic cell death in collagen-induced arthritis mouse models, Nat. Commun. 13 (1) (2022) 676. https://doi.org/10.1038/s41467-021-27948-4.

[6] L. Cao, S. Zhao, K. Han, et al., Managing ferroptosis-related diseases with indirect dietary modulators of ferroptosis, J. Nutr. Biochem. 120 (2023) 109427. https://doi.org/10.1016/j.jnutbio.2023.109427.

[7] S. Bieri, B. Moller, J. Amsler, Ferroptosis in arthritis: driver of the disease or therapeutic option? Int. J. Mol. Sci. 25(15) (2024) 8212. https://doi.org/10.3390/ijms25158212.

[8] Y. Aihaiti, H. Zheng, Y. Cai, et al., Exploration and validation of therapeutic molecules for rheumatoid arthritis based on ferroptosis-related genes, Life Sci. 351 (2024) 122780. https://doi.org/10.1016/j.lfs.2024.122780.

[9] Z. Liu, R. Kang, N. Yang, et al., Tetrahydrobiopterin inhibitor-based antioxidant metabolic strategy for enhanced cancer ferroptosis-immunotherapy, J. Colloid. Interface Sci. 658 (2024) 100-113. https://doi.org/10.1016/j.jcis.2023.12.042.

[10] C. Zhao, Y. Yu, G. Yin, et al., Sulfasalazine promotes ferroptosis through AKT-ERK1/2 and P53-SLC7A11 in rheumatoid arthritis, Inflammopharmacology 32(2) (2024) 1277-1294. https://doi.org/10.1007/s10787-024-01439-6.

[11] H. Shi, B. Hou, H. Li, et al., Cyclophosphamide induces the ferroptosis of tumor cells through heme oxygenase-1, Front. Pharmacol. 13 (2022) 839464. https://doi.org/10.3389/fphar.2022.839464.

[12] H. Zhao, C. Tang, M. Wang, et al., Ferroptosis as an emerging target in rheumatoid arthritis, Front. Immunol. 14 (2023) 1260839. https://doi.org/10.3389/fimmu.2023.1260839.

[13] L. Long, H. Guo, X. Chen, et al., Advancement in understanding the role of ferroptosis in rheumatoid arthritis, Front. Physiol. 13 (2022) 1036515. https://doi.org/10.3389/fphys.2022.1036515.

[14] C.D. Buckley, C. Ospelt, S. Gay, et al., Location, location, location: how the tissue microenvironment affects inflammation in RA, Nat. Rev. Rheumatol. 17(4) (2021) 195-212. https://doi.org/10.1038/s41584-020-00570-2.

[15] J. Majnik, N. Csaszar-Nagy, G. Bocskei, et al., Non-pharmacological treatment in difficult-to-treat rheumatoid arthritis, Front. Med. 9 (2022) 991677. https://doi.org/10.3389/fmed.2022.991677.

[16] K.F. Zhai, H. Duan, C.Y. Cui, et al., Liquiritin from glycyrrhiza uralensis attenuating rheumatoid arthritis *via* reducing inflammation, suppressing angiogenesis, and inhibiting MAPK signaling pathway, J. Agric. Food. Chem. 67(10) (2019) 2856-2864. https://doi.org/10.1021/acs.jafc.9b00185.

[17] K.F. Zhai, H. Duan, Y. Chen, et al., Apoptosis effects of imperatorin on synoviocytes in rheumatoid arthritis through mitochondrial/Caspase-mediated pathways, Food. Funct. 9(4) (2018) 2070-2079. https://doi.org/10.1039/c7fo01748k.

[18] L. Xiong, T. Luo, L.F. Wang, et al., Potential of food protein-derived peptides for the improvement of osteoarthritis, Trends. Food. Sci. Tech. 129 (2022) 544-557. https://doi.org/10.1016/j.tifs.2022.10.007.

[19] M. Kohno, Soybean protein and peptide as complementation medical food materials for treatment of dyslipidemia and inflammatory disorders, Food. Sci. Technol. Res. 23(6) (2017) 773-782. https://doi.org/10.3136/fstr.23.773.

[20] J. Felim, C.K. Chen, D. Tsou, et al., Effect of different collagen on anterior cruciate ligament transection and medial meniscectomy-induced osteoarthritis male rats, Front. Bioeng. Biotechnol. 10 (2022) 917474. https://doi.org/10.3389/fbioe.2022.917474.

[21] C. Xue, W. Pan, X. Lu, et al., Effects of compound deer bone extract on osteoporosis model mice and intestinal microflora, J. Food. Biochem. 45(6) (2021) e13740. https://doi.org/10.1111/jfbc.13740.

[22] H. Lee, Y. Park, A.C. Won, et al., Deer bone extract suppresses articular cartilage damage induced by monosodium iodoacetate in osteoarthritic rats: an *in vivo* micro-computed tomography study, J. Med. Food. 17(6) (2014) 701-706. https://doi.org/10.1089/jmf.2013.3015.

[23] X. Liu, X. Chen, C. Zhang, et al., Mitochondrion-NLRP3 inflammasome activation in macrophages: a novel mechanism of the anti-inflammatory effect of notopterygium in rheumatoid arthritis treatment, Biomed. Pharmacother. 167 (2023) 115560. https://doi.org/10.1016/j.biopha.2023.115560.

[24] Q. Li, F. Peng, X. Yan, et al., Inhibition of SLC7A11-GPX4 signal pathway is involved in aconitine-induced ferroptosis *in vivo* and *in vitro*, J. Ethnopharmacol. 303 (2023) 116029. https://doi.org/10.1016/j.jep.2022.116029.

[25] Y. Miao, Y. Chen, F. Xue, et al., Contribution of ferroptosis and GPX4's dual functions to osteoarthritis progression, eBioMedicine 76 (2022) 103847. https://doi.org/10.1016/j.ebiom.2022.103847.

[26] Y. Lu, J. Min, Y. Jin, et al., Quantitative analysis of deer bone hydroethanolic extract using label-free proteomics: investigating its safety and promoting effect on mouse embryonic osteoblastic progenitor cell proliferation, Nutrients 16(22) (2024) 3807. https://doi.org/10.3390/nu16223807.

[27] C. Glorieux, S. Liu, D. Trachootham, et al., Targeting ROS in cancer: rationale and strategies, Nat. Rev. Drug. Discov. 23(8) (2024) 583-606. https://doi.org/10.1038/s41573-024-00979-4.

[28] W. Zhao, P. Zhuang, Y. Chen, et al., "Double-edged sword" effect of reactive oxygen species (ROS) in tumor development and carcinogenesis, Physiol. Res. 72(3) (2023) 301-307. https://doi.org/10.33549/physiolres.935007.

[29] K.F. Zhai, H. Duan, G.J. Khan, et al., Salicin from alangium chinense ameliorates rheumatoid arthritis by modulating the Nrf2-HO-1-ROS pathways, J. Agric. Food. Chem. 66(24) (2018) 6073-6082. https://doi.org/10.1021/acs.jafc.8b02241.

[30] X. Bao, Validation of new immune and inflammation-related diagnostic biomarkers for RA, Clin. Rheumatol. 43(3) (2024) 949-958. https://doi.org/10.1007/s10067-024-06882-y.

[31] V. Vasudevan, P. Agnihotri, S. Biswas, Post translational modification and its pathologic association in rheumatoid arthritis: a brief perspective, Curr. Protein. Pept. Sci. 22(7) (2021) 548-558. https://doi.org/10.2174/1389203722666210215152433.

[32] C. Gioia, B. Lucchino, M.G. Tarsitano, et al., Dietary habits and nutrition in rheumatoid arthritis: can diet influence disease development and clinical manifestations? Nutrients 12(5) (2020) 1456. https://doi.org/10.3390/nu12051456.

[33] J. Wang, C. Liu, T. Wang, et al., Single-cell communication patterns and their intracellular information flow in synovial fibroblastic osteoarthritis and rheumatoid arthritis, Immunol. Lett. 263 (2023) 1-13. https://doi.org/10.1016/j.imlet.2023.09.005.

[34] Z. Ouyang, L. Dong, F. Yao, et al., Cartilage-related collagens in osteoarthritis and rheumatoid arthritis: from pathogenesis to therapeutics, Int. J. Mol. Sci. 24(12) (2023) 9841. https://doi.org/10.3390/ijms24129841.

[35] G. Zhao, Y. Liu, Y. Zheng, et al., Exploring molecular mechanisms of intra-articular changes in osteonecrosis of femoral head using DIA proteomics and bioinformatics, J. Orthop. Surg. Res. 19(1) (2024) 13. https://doi.org/10.1186/s13018-023-04464-3.

[36] M. Sun, Q. Wang, J. Huang, et al., Asiatic acid induces ferroptosis of RA-FLSs *via* the Nrf2/Hmox1 pathway to relieve inflammation in rheumatoid arthritis, Int. Immunopharmacol. 137 (2024) 112394. https://doi.org/10.1016/j.intimp.2024.112394.

[37] J. Chen, G. Zhu, S. Sun, et al., 7-Deacetyl-gedunin suppresses proliferation of human rheumatoid arthritis synovial fibroblast through activation of Nrf2/ARE signaling, Int. Immunopharmacol. 107 (2022) 108557. https://doi.org/10.1016/j.intimp.2022.108557.

[38] X. Gao, N. Guo, H. Xu, et al., Ibuprofen induces ferroptosis of glioblastoma cells *via* downregulation of nuclear factor erythroid 2-related factor 2 signaling pathway, Anti-Cancer Drugs 31(1) (2020) 27-34. https://doi.org/10.1097/CAD.0000000000000825.

[39] C. Yan, F. Xuan, Paris saponin VII promotes ferroptosis to inhibit breast cancer via Nrf2/GPX4 axis, Biochem. Biophys. Res. Commun. 697 (2024) 149524. https://doi.org/10.1016/j.bbrc.2024.149524.

[40] L. Ibrahim, C. Stanton, K. Nutsch, et al., Succinylation of a KEAP1 sensor lysine promotes Nrf2 activation, Cell. Chem. Biol. 30(10) (2023) 1295-1302. https://doi.org/10.1016/j.chembiol.2023.07.014.

[41] L. Zeng, W. Zhao, T. Han, et al., Ropivacaine prompts ferroptosis to enhance the cisplatin-sensitivity of human colorectal cancer through SIRT1/Nrf2 signaling pathway, Chem. Biol. Interact. 400 (2024) 111163. https://doi.org/10.1016/j.cbi.2024.111163.

[42] X. Gao, W. Hu, D. Qian, et al., The mechanisms of ferroptosis under hypoxia, Cell. Mol. Neurobiol. 43(7) (2023) 3329-3341. https://doi.org/10.1007/s10571-023-01388-8.

[43] A. Cuadrado, A.I. Rojo, G. Wells, et al., Therapeutic targeting of the Nrf2 and KEAP1 partnership in chronic diseases, Nat. Rev. Drug. Discov. 18(4) (2019) 295-317. https://doi.org/10.1038/s41573-018-0008-x.

[44] C. Wang, M. Leng, C. Ding, et al., Ferritinophagy-mediated ferroptosis facilitates methotrexate-induced hepatotoxicity by high-mobility group box 1 (HMGB1), Liver. Int. 44(3) (2024) 691-705. https://doi.org/10.1111/liv.15811.

[45] J. Chen, J. Wang, C. Li, et al., Dexmedetomidine reverses MTX-induced neurotoxicity and inflammation in hippocampal HT22 cell lines *via* NCOA4-mediated ferritinophagy, Aging (Albany NY) 13(4) (2021) 6182-6193. https://doi.org/10.18632/aging.202626.

[46] S. Chang, M. Tang, B. Zhang, et al., Ferroptosis in inflammatory arthritis: a promising future, Front. Immunol. 13 (2022) 955069. https://doi.org/10.3389/fimmu.2022.955069.